

Giant Spin Gap and Magnon Localization in the Disordered Heisenberg Antiferromagnet $\text{Sr}_2\text{Ir}_{1-x}\text{Ru}_x\text{O}_4$

Yue Cao,^{1,*} Xuerong Liu,^{2,†} Wenhui Xu,^{1,‡} Weiguo Yin,¹ D. Meyers,¹ Jungho Kim,³ Diego Casa,³ Mary Upton,³ Thomas Gog,³ Tom Berlijn,⁴ Gonzalo Alvarez,⁴ Shujuan Yuan,⁵ Jasminka Terzic,⁵ J. M. Tranquada,¹ John P. Hill,⁶ Gang Cao,^{5,7} Robert M. Konik,¹ and M. P. M. Dean^{1,§}

¹*Condensed Matter Physics and Material Science Department,
Brookhaven National Laboratory, Upton, NY 11973*

²*Institute of Physics, Chinese Academy of Sciences, Beijing 100190, China*

³*Advanced Photon Source, Argonne National Laboratory, Lemont, IL 60439, U.S.A.*

⁴*Computer Science and Mathematics Division and Center for Nanophase Materials Sciences,
Oak Ridge National Laboratory, Oak Ridge, TN 37831, U. S. A.*

⁵*Department of Physics and Astronomy, University of Kentucky, Lexington, KY*

⁶*National Synchrotron Light Source II (NSLS-II),
Brookhaven National Laboratory, Upton, NY 11973*

⁷*Department of Physics, University of Colorado at Boulder, Boulder, CO 80309*

(Dated: August 25, 2016)

We study the evolution of magnetic excitations in the disordered two-dimensional antiferromagnet $\text{Sr}_2\text{Ir}_{1-x}\text{Ru}_x\text{O}_4$. A gigantic magnetic gap greater than 40 meV opens at $x = 0.27$ and increases with Ru concentration, rendering the dispersive magnetic excitations in Sr_2IrO_4 almost momentum-independent. Up to a Ru concentration of $x = 0.77$, both experiments and first-principles calculations show the Ir $J_{\text{eff}} = 1/2$ state remains intact. The magnetic gap arises from the local interaction anisotropy in the proximity of the Ru disorder. Under the coherent potential approximation, we reproduce the experimental magnetic excitations using the disordered Heisenberg antiferromagnetic model with suppressed next-nearest neighbor ferromagnetic coupling.

PACS numbers: 71.15.Mb, 71.45.Gm, 75.10.Nr, 78.70.Ck, 78.70.En

Many of the most interesting phases in condensed matter are accessed by chemically substituting (that is, doping) well-ordered crystalline materials. A particularly notable example is high temperature superconductivity in the cuprates which arises when the quasi-two-dimensional (2D) antiferromagnetic Mott insulating phase in the parent compounds is suppressed. For this reason, understanding the behavior of antiferromagnets in different doping regimes has become a quintessential problem in quantum magnetism [1–5]. The majority of experimental work [6–9] has focused on out-of-plane chemical substitutions that simultaneously introduce mobile carriers and weak disorder [10]. In-plane substitutions introduce strong disorder effects and may or may not change the itinerant carrier concentration. Such a situation is less understood [11], and in particular, there is very little information about how magnetic dynamics change upon high doping levels, for example, close to the geometrical percolation threshold $\sim 40\%$ above which magnetic patches are disconnected [3].

The layered iridate Sr_2IrO_4 has recently emerged as a novel antiferromagnetic insulator with close structural and electronic analogies to the cuprates [12–15]. Furthermore, single crystals of $\text{Sr}_2\text{Ir}_{1-x}\text{M}_x\text{O}_4$ can be produced where Ir is substituted with a different transition metal M over a wide range [16–20]. This, combined with recent progress in applying resonant inelastic X-ray scattering (RIXS) [9, 21] to iridates [22–26] provides an excellent opportunity to determine the behavior of magnetic cor-

relations in disordered (pseudo)spin-1/2 Heisenberg antiferromagnets.

In this *Letter*, we investigate the evolution of magnetic excitations in the heavily disordered regime of $\text{Sr}_2\text{Ir}_{1-x}\text{Ru}_x\text{O}_4$. The magnetic correlations survive at least to a high Ru doping of $x = 0.77$. A magnetic gap greater than 40 meV develops as early as $x = 0.27$, and increases with higher Ru dopings. Eventually the magnetic excitations become localized, and non-dispersive throughout the Brillouin zone. We present a quantitative description of the observed antiferromagnetic excitations using density functional theory and coherent potential approximation (CPA). The giant magnetic gap and the flattened magnetic excitations originate from local orbital anisotropy, as well as the suppression of next-nearest neighbor magnetic interactions.

Single crystals of $\text{Sr}_2\text{Ir}_{1-x}\text{Ru}_x\text{O}_4$ were grown from off-stoichiometric quantities of SrCl_2 , SrCO_3 , IrO_2 , and RuO_2 using self-flux techniques [18]. Fig. 1 (a) shows the magnetic behavior of $\text{Sr}_2\text{Ir}_{1-x}\text{Ru}_x\text{O}_4$ which undergoes a cross-over from antiferromagnetic (AFM) to paramagnetic (PM) around $x \sim 0.50$. Further information on sample growth and characterizations are provided in Ref. [18] and the Supplementary Information [27].

The RIXS measurements were performed at the Ir L_3 -edge using the MERIX endstation (27-ID-B) at the Advanced Photon Source, Argonne National Laboratory, with a total energy resolution of 80 meV (full width at half maximum) and momentum resolution of 0.23\AA^{-1} .

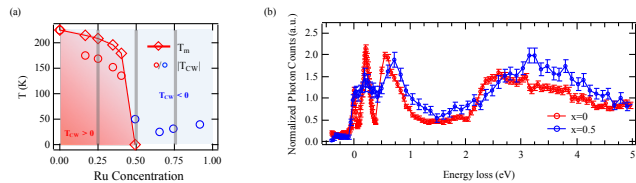


FIG. 1. (Color online) (a) The magnetic phase diagram of $\text{Sr}_2\text{Ir}_{1-x}\text{Ru}_x\text{O}_4$. T_m is the onset temperature for an increased magnetization under an external field of 0.1 T. Around $x = 0.50$, T_m is suppressed to zero. This is also where the Curie-Weiss temperature, T_{C-W} , changes sign [18]. Grey bars mark the select Ru concentrations studied in this work. (b) RIXS spectra of Sr_2IrO_4 and $\text{Sr}_2\text{Ir}_{0.5}\text{Ru}_{0.5}\text{O}_4$ at $(\pi, 0)$ over a 5.5 eV window, showing persistent excitations centered around 200 meV, 700 meV and 3.5 eV. These are assigned to magnetic, intra- t_{2g} and $t_{2g} \rightarrow e_g$ processes respectively.

All data presented were taken at the base temperature of the cryostat ~ 12 K. Figure 1 (b) plots RIXS spectra of $\text{Sr}_2\text{Ir}_{1-x}\text{Ru}_x\text{O}_4$ over a wide energy window up to 5 eV. There are three distinctive energy-loss features, around 200 meV, 700 meV, and 3.5 eV, respectively. The latter two peaks are orbital excitations of the hole in the valence band, providing information on the electronic configuration of the doped and parent compounds. Specifically, the 3.5 eV peak corresponds to the $t_{2g} \rightarrow e_g$ excitation. Its increase in energy with Ru concentration is consistent with what is expected due to structural changes. Going from $x = 0$ to $x = 0.50$ doping, the Ir-O octahedra elongate by 1.0% along the apex, and contract by 2.9% in-plane [18], increasing the crystal field splitting, and moving the $t_{2g} \rightarrow e_g$ feature to higher energies. By comparing to Sr_2IrO_4 , we assign the energy-loss peak around 700 meV to the intra- t_{2g} transition, or more precisely, the transition between the Ir $5d$ $J_{\text{eff}} = 1/2$ and $J_{\text{eff}} = 3/2$ states [22, 23]. By the same token, we deem the energy-loss peak around 200 meV as magnetic in nature, arising from the pseudospin flip.

With increasing Ru concentration all three peaks persist with comparable energy-scales. Thus the Ir electronic configuration does not change dramatically, and the $J_{\text{eff}} = 1/2$ and $J_{\text{eff}} = 3/2$ states are still present at these higher Ru concentrations. In Sr_2IrO_4 and Sr_2RuO_4 , Ir^{4+} and Ru^{4+} have formal electron configurations of $5d^5$ and $4d^4$, respectively. As dc-resistivity reduces with Ru concentration [18], one might naïvely assume that the numbers of d -electrons on Ru and Ir get closer to an average of 4.5, due to increased electron itinerancy. This would indicate effective hole doping on the Ir site into the $J_{\text{eff}} = 1/2$ level, with drastic changes in the local electronic structure. In contrast, our data seem to suggest that Ir maintains a formal valence of 4^+ , which we will now examine using first-principles calculations.

We calculate the orbital configuration of

Ru concentration		0%	25%	50%	100%
Ir	NM	5.20	5.16	5.19	
	SP	5.20	5.19	5.21	
Ru	NM		4.53	4.61	4.47
	SP		4.58	4.47	4.46

TABLE I. The number of d electrons on each Ir/Ru site, derived from GGA+ U calculations. We used $U = 2$ eV [12] for Ir and $U = 3$ eV for Ru. NM and SP stand for the non-magnetic and spin-polarized calculations respectively.

$\text{Sr}_2\text{Ir}_{1-x}\text{Ru}_x\text{O}_4$ in the GGA+ U implementation of the density functional theory [27]. Table I lists the calculated electron occupation number on the Ir and Ru d -orbitals vs. Ru concentration. Up to $x > 0.75$ the numbers of d -electrons on Ir/Ru have relatively small changes compared to the doped Ru concentration, especially when a spin-polarized ground state is considered. Thus both Ir/Ru sites maintain a valence close to 4^+ , similar to those in $\text{Sr}_2\text{IrO}_4/\text{Sr}_2\text{RuO}_4$, in agreement with the X-ray absorption experiments in Ref. [19]. We project the d electron density of states onto the Ir/Ru orbitals, and find that the $J_{\text{eff}} = 1/2$ and $J_{\text{eff}} = 3/2$ are indeed robust. This is because for each individual Ir-O octahedron, the spin-orbit coupling energy scale [12, 28] (~ 400 meV) dominates over the tetragonal splitting between t_{2g} levels, giving rise to a relatively well-defined pseudospin-1/2 state [28, 29]. This interpretation also agrees with the persistence of the insulating phase up to $x \simeq 0.50$ in $\text{Sr}_2\text{Ir}_{1-x}\text{Ru}_x\text{O}_4$ [18]. In our calculation, the electrons near the Fermi level come primarily from the local Ru-O octahedra, and cannot move freely especially for low Ru concentrations. GGA+ U calculations for all Ru concentrations favor spin-polarized ground-states, with antiferromagnetic couplings between the nearest-neighbor Ir $J_{\text{eff}} = 1/2$ and Ru $s = 1$ (pseudo-)spins. We therefore consider that the effect of Ru doping in $\text{Sr}_2\text{Ir}_{1-x}\text{Ru}_x\text{O}_4$ is primarily to introduce substitutional $s = 1$ magnetic disorder (rather than charge doping) for a large range of Ru concentration (until the material gets sufficiently close to Sr_2RuO_4). We show later that phenomenological CPA simulations, based on this picture, account for the observed magnetic dispersion.

In Fig. 2(a)-(c) we take a closer look at the excitations within the first 1.5 eV of energy loss as $\text{Sr}_2\text{Ir}_{1-x}\text{Ru}_x\text{O}_4$ crosses the AFM-PM phase boundary: (a) $x = 0.27$, (b) $x = 0.50$, and (c) $x = 0.77$. All dopings are marked with grey bars in the phase diagram in Fig. 1 (a). We assign the $(\pi, 0)$ direction to be parallel to the nearest neighbor Ir-Ir bond directions, in analogy with the usual definition in square-net cuprates. As expected in a disordered system, both the magnetic and orbital excitations are broader than in the undoped Sr_2IrO_4 . We fit the elastic

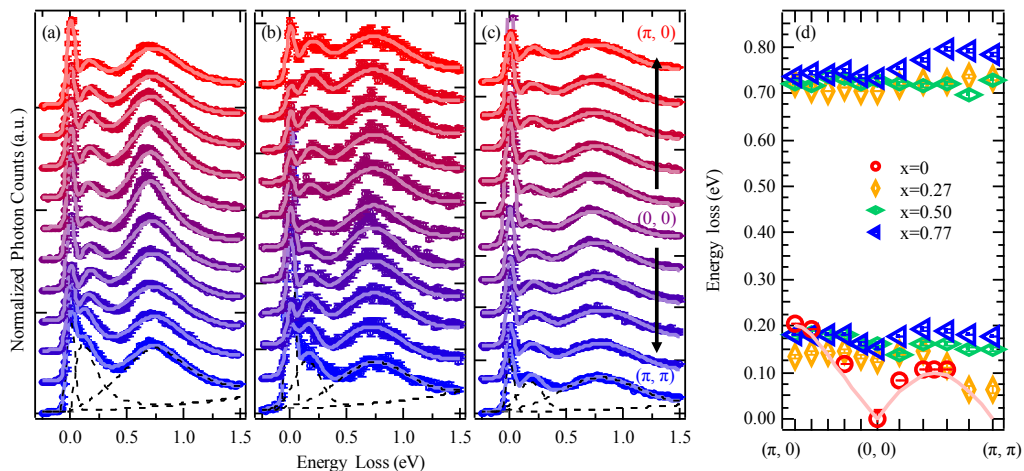


FIG. 2. (Color online) (a)-(c) The energy-loss spectra along $(\pi, 0) \rightarrow (0, 0) \rightarrow (\pi, \pi)$ high symmetry directions for three Ru dopings (a) $x = 0.27$, (b) $x = 0.50$, and (c) $x = 0.77$. The solid thick lines are fits to the RIXS data. The dashed black curves are the individual components of the fit for the energy loss curve at (π, π) . (d) Energies of the magnetic and orbital excitations as a function of momentum transfer for different Ru concentrations. Error bars represent the uncertainty from the least-mean square fitting algorithm. The pink solid line is the fitted magnon dispersion in Sr_2IrO_4 reproduced from Ref. [22].

peak and the two excitations with three Gaussian peaks on top of a smooth background, and the fitted energies of the magnetic and orbital modes are shown in Fig. 2 (d).

The most striking feature is that the antiferromagnetic excitations persist up to at least $x = 0.77$, and that the maximum energy scale of the magnetic excitations at high dopings is comparable to that in undoped Sr_2IrO_4 . In a simple mean-field description, the overall magnetic excitation energy would be expected to decrease appreciably due to lower magnon energies in Sr_2RuO_4 . The results here reflect the strong local correlation in the material that voids mean-field descriptions. Such a result is reminiscent of studies of electron and hole doped cuprates and iridates [6–9, 24, 25, 30–32], albeit up to smaller maximum doping level of 40% in cuprates and a mere 10% in iridates. Specifically, the magnetic excitation energies at $(\pi, 0)$ are robust against doped charge carriers and in this work disorder, while profound changes take place around e.g. (π, π) and $(\pi/2, \pi/2)$ [7, 8, 24, 25, 33]. This similarity is not necessarily expected as it involves comparing the effects of itinerant carriers introduced by out-of-plane atomic substitutions with in-plane replacement of the Ir atoms.

The second observation is that a large spin gap already opens for $x = 0.27$, and appears to increase and saturate with Ru doping across the phase transition. This is in sharp contrast to the dispersive, almost gapless paramagnetic excitations in the electron and hole doped cuprates and iridates mentioned above. At higher doping of $x = 0.50$ and $x = 0.77$, the magnetic modes are almost dispersionless within an energy range of 150–180 meV. Such an energy scale lies between the zone

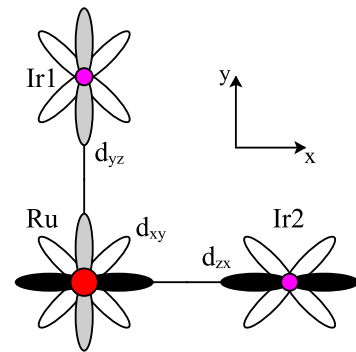


FIG. 3. (Color online) Geometry of Ru-Ir bonds with orbitals active t_{2g} orbitals along these bonds (top view). Black: d_{zx} orbitals. Grey: d_{yz} orbitals. White: d_{xy} orbitals. The oxygen atoms between the nearest-neighbor Ir atoms are not displayed, and the oxygen states have been projected out in the effective superexchange model.

boundary energy-scales of Sr_2IrO_4 : ~ 200 meV at $(\pi, 0)$ and ~ 100 meV at $(\pi/2, \pi/2)$.

The opening up of a finite gap in the spin excitation spectrum can be explained by broken continuous rotational symmetry. In our case, a plausible origin of spin gap is the anisotropic antiferromagnetic exchange between t_{2g} electrons experiencing different spin-orbit coupling on the Ru $4d$ and Ir $5d$ orbitals [34], as well as the strong Hund's coupling on the Ru $4d$ orbitals. We illustrate this by considering the toy model in Fig. 3. For a pair of Ru-Ir spins, after projecting out the oxygen states, the effective magnetic Hamiltonian $\mathcal{H} = \mathcal{H}_{\text{SO}} + \mathcal{H}_{\text{Hund}} + \mathcal{H}_{\text{AF}}$ consists of the spin-orbit

coupling \mathcal{H}_{SO} on the Ir sites, the Hund's coupling $\mathcal{H}_{\text{Hund}}$ between the t_{2g} spins on the Ru site, and the antiferromagnetic coupling between Ru and Ir spins, $\mathcal{H}_{\text{AF}} = J_{yz}\mathbf{s}_{\text{Ru},yz} \cdot \mathbf{s}_{\text{Ir1},yz} + J_{xy}\mathbf{s}_{\text{Ru},xy} \cdot \mathbf{s}_{\text{Ir1},xy} + J_{zx}\mathbf{s}_{\text{Ru},zx} \cdot \mathbf{s}_{\text{Ir2},zx} + J_{xy}\mathbf{s}_{\text{Ru},xy} \cdot \mathbf{s}_{\text{Ir2},xy}$. As a first-order perturbation to \mathcal{H}_{SO} , \mathcal{H}_{AF} induces an effective anisotropic coupling between the t_{2g} spins on Ru and the pseudospin (instead of physical spin) \mathbf{J}_{eff} on Ir [34]. For example, the effective coupling on the Ru-Ir2 bond, $\mathcal{H}_{\text{AF2}} = J_{zx}/3(s_{\text{Ru},zx}^x J_{\text{Ir2, eff}}^x - s_{\text{Ru},zx}^y J_{\text{Ir2, eff}}^y + s_{\text{Ru},zx}^z J_{\text{Ir2, eff}}^z) + J_{xy}/3(s_{\text{Ru},xy}^x J_{\text{Ir2, eff}}^x + s_{\text{Ru},xy}^y J_{\text{Ir2, eff}}^y + s_{\text{Ru},xy}^z J_{\text{Ir2, eff}}^z)$, has an easy $z-x$ plane. Similarly, the effective coupling on the Ru-Ir1 bond has an easy $y-z$ plane. The Hund's coupling on the Ru site, $\mathcal{H}_{\text{Hund}} = -J_H \mathbf{S}_{\text{Ru}}^2$, where $\mathbf{S}_{\text{Ru}} = \mathbf{s}_{\text{Ru},xy} + \mathbf{s}_{\text{Ru},yz} + \mathbf{s}_{\text{Ru},zx}$ favors aligning the Ru t_{2g} spins. If one Ru site is connected to neighboring Ir sites by at least two perpendicular Ru-Ir bonds (as in Fig. 3), the degeneracy of rotating $\mathbf{s}_{\text{Ru},yz}$ in the $y-z$ plane and $\mathbf{s}_{\text{Ru},zx}$ in the $z-x$ plane will be lifted by $\mathcal{H}_{\text{Hund}}$, giving rise to the effective anisotropic exchange with an easy z -axis.

We capture the geometrical impact of introducing spin disorder and spin anisotropy on the system using the coherent potential approximation (CPA) [35, 36] following the recipe in Ref. [36], and calculate the magnetic excitation spectrum (Fig. 4) [37]. The nearest neighbor (NN) coupling between Ir sites is selected to be $J_{\text{Ir-Ir}} = 60$ meV, identical to that in Sr_2IrO_4 . We extract nearest-neighbor Ir-Ru coupling $J_{\text{Ir-Ru}} \simeq 60$ meV, from the energy differences between the magnetic and paramagnetic groundstates calculated using GGA+ U . Other input exchange energies for the CPA calculation includes the exchange between next (NNN) and next-next nearest (NNNN) neighboring $J_{\text{eff}} = 1/2$ pseudospins, $J'_{\text{Ir-Ir}} = -20$ meV, and $J''_{\text{Ir-Ir}} = 15$ meV, respectively [22, 23]. As to the exchange between NN $s = 1$ spins, there is no qualitative change in the simulated magnetic excitation for a weak antiferromagnetic $J_{\text{Ru-Ru}} \lesssim 5$ meV. Fig. 4 (a) and (b) show increased magnetic gaps at $(0,0)$ and (π,π) with rising $s = 1$ concentrations. At $x = 0.50$ in Fig. 4 (b), the magnetic excitations are damped and flattened around much of the Brillouin zone, except along $(\pi,0)-(0,0)$ where the excitation spectrum is barely affected by the disorder. To further increase the simulated magnetic gap, we set $J'_{\text{Ir-Ir}}$ and $J''_{\text{Ir-Ir}}$ to zero, and the calculations are shown in Fig. 4 (c). The magnetic excitation is turned into a heavily damped localized mode, recapturing the dispersionless feature in Fig. 2 (d). Our suppression of the NNN and NNNN exchange energies may reflect that the corresponding magnetic couplings are destroyed geometrically in the presence of more $s = 1$ disorders.

The magnetic excitation energies at the two centers of the antiferromagnetic Brillouin zone $(0,0)$ and (π,π) are not identical in the $x = 0.27$ sample, unlike those in the Sr_2IrO_4 (Fig. 2 (d), also see Ref. [22, 23]). The

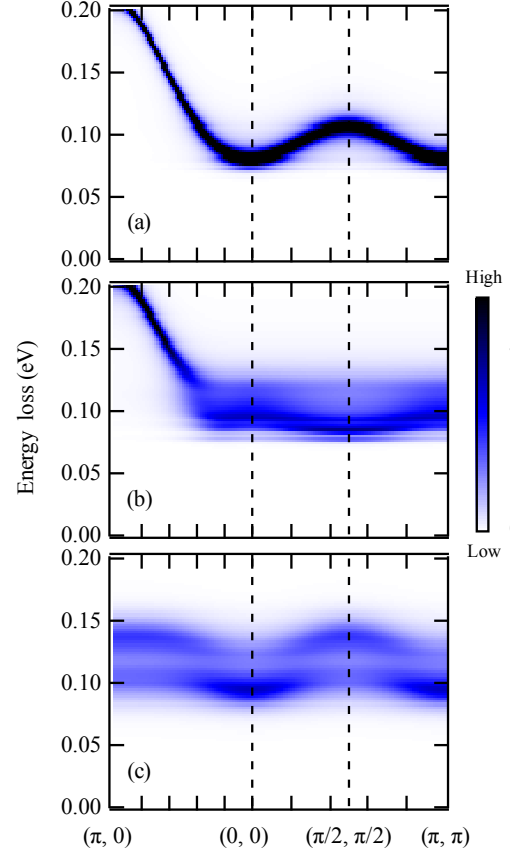


FIG. 4. (Color online) (a) and (b) Magnetic excitations calculated using CPA with (a) $x = 0.25$ and (b) $x = 0.50$ concentrations of $s = 1$ moments (to simulate the Ru sites), preserving both the nearest neighbor (NN) and next-nearest neighbor (NNN) magnetic interactions between $J_{\text{eff}} = 1/2$ sites. (c) Calculated magnetic excitations with 50% $s = 1$ moments. The couplings between the NNN and further $J_{\text{eff}} = 1/2$ moments are suppressed.

observed inequivalence may signal a breakdown of the antiferromagnetic Brillouin zone, which is well-defined *only* under translation symmetry. Admittedly, this effect is not captured in the current CPA calculation. However, in the carrier-doped Mott insulators, where the antiferromagnetic Brillouin zone is also ill-defined, there are theoretical proposals showing different magnetic excitation energies at $(0,0)$ and (π,π) . For example, using more rigorous determinant quantum Monte Carlo methods, Jia *et al.* [5] interpreted the meltdown of the antiferromagnetic Brillouin zone as associated to the change in spin correlation from antiferromagnetic to ferromagnetic. Such an effect can also be shown in the Schwinger boson treatment of the square-lattice quantum antiferromagnet using the ferromagnetic configuration instead of the Néel state as the reference state, in which the long-range antiferromagnetic order is generated via Bose-Einstein condensation at (π,π) with a considerable spin gap at $(0,0)$ [38]. It is

to be noted that the antiferromagnetic and/or structural Brillouin zone also fails to describe the complete electronic structures in (effectively) carrier doped Sr_2IrO_4 , as observed in angle-resolved photoemission experiments [15, 39, 40].

In summary, we have measured the magnetic excitations in $\text{Sr}_2\text{Ir}_{1-x}\text{Ru}_x\text{O}_4$ across a wide doping range and observed a cross-over from dispersive to gapped, localized magnons. First-principles calculations and simulations using the coherent potential approximation provide a thorough description of these findings based on disorder and local anisotropy effects. Similar effects are likely to be at play in other heavily doped transition metal oxides with important implications for understanding the importance of disorder on magnetic correlations and how this might relate to emergent phenomena such as high-Tc superconductivity.

The authors acknowledge fruitful discussions with Gilberto Fabbri and Daniel Haskel. The work at Brookhaven National Laboratory was supported by the U. S. Department of Energy, Division of Materials Science, under Contract No. de-sc0012704. X.R.L. receives financial support from MOST (No. 2015CB921302), CAS (Grant No: XDB07020200), and by the National Thousand Young-Talents Program of China. T. B. and G. A. received funding from the Center for Nanophase Materials Sciences, sponsored by the Scientific User Facilities Division, Basic Energy Sciences, Department of Energy (DOE), USA, under contract with UT-Battelle. The work at the University of Kentucky was supported by NSF through Grant DMR-1265162. This research used Sector 27 of the Advanced Photon Source, a U.S. Department of Energy (DOE) Office of Science User Facility operated for the DOE Office of Science by Argonne National Laboratory under Contract No. DE-AC02-06CH11357 and beamline X22C of the National Synchrotron Light Source, a U.S. Department of Energy (DOE) Office of Science User Facility operated for the DOE Office of Science by Brookhaven National Laboratory under Contract No. DE-AC02-98CH10886.

* ycao@bnl.gov

† xliu@aphy.iphy.ac.cn

‡ wenhuxu@bnl.gov

§ mdean@bnl.gov

- [1] S. Sachdev, C. Buragohain, and M. Vojta, *Science* **286**, 2479 (1999).
- [2] P. A. Lee, N. Nagaosa, and X.-G. Wen, *Rev. Mod. Phys.* **78**, 17 (2006).
- [3] O. P. Vajk, P. K. Mang, M. Greven, P. M. Gehring, and J. W. Lynn, *Science* **295**, 1691 (2002).
- [4] D. J. Scalapino, *Rev. Mod. Phys.* **84**, 1383 (2012).
- [5] C. J. Jia, E. A. Nowadnick, K. Wohlfeld, Y. F. Kung, C.-C. Chen, S. Johnston, T. Tohyama, B. Moritz, and T. P. Devereaux, *Nat. Commun.* **5**, 3314 (2014).
- [6] M. P. M. Dean, G. Dellea, R. S. Springell, F. Yakhou-Harris, K. Kummer, N. B. Brookes, X. Liu, Y. J. Sun, J. Strle, T. Schmitt, *et al.*, *Nat. Mater.* **12**, 1019 (2013).
- [7] K. Ishii, M. Fujita, T. Sasaki, M. Minola, G. Dellea, C. Mazzoli, K. Kummer, G. Ghiringhelli, L. Braicovich, T. Tohyama, *et al.*, *Nat. Commun.* **5**, 3714 (2014).
- [8] W. S. Lee, J. J. Lee, E. A. Nowadnick, S. Gerber, W. Tabis, S. W. Huang, V. N. Strocov, E. M. Motoyama, G. Yu, B. Moritz, *et al.*, *Nat. Phys.* **10**, 883 (2014).
- [9] M. P. M. Dean, J. Magn. Magn. Mater. **376**, 3 (2015).
- [10] H. Alloul, J. Bobroff, M. Gabay, and P. J. Hirschfeld, *Rev. Mod. Phys.* **81**, 45 (2009).
- [11] Calculations on spin excitations and long-range order in diluted quantum antiferromagnets were presented in, e.g., A. L. Chernyshev, Y.-C. Chen, and A. H. Castro Neto, *Phys. Rev. Lett.* **87**, 067209 (2001); A. L. Chernyshev, Y.-C. Chen, and A. H. Castro Neto, *Phys. Rev. B* **65**, 104407 (2002).
- [12] B. J. Kim, H. Jin, S. J. Moon, J.-Y. Kim, B.-G. Park, C. S. Leem, J. Yu, T. W. Noh, C. Kim, S.-J. Oh, *et al.*, *Phys. Rev. Lett.* **101**, 076402 (2008).
- [13] B. J. Kim, H. Ohsumi, T. Komesu, S. Sakai, T. Morita, H. Takagi, and T. Arima, *Science* **323**, 1329 (2009).
- [14] Y. K. Kim, O. Krupin, J. D. Denlinger, A. Bostwick, E. Rotenberg, Q. Zhao, J. F. Mitchell, J. W. Allen, and B. J. Kim, *Science* **345**, 187 (2014).
- [15] Y. Cao, Q. Wang, J. A. Waugh, T. J. Reber, H. Li, X. Zhou, S. Parham, S.-R. Park, N. C. Plumb, E. Rotenberg, A. Bostwick, *et al.*, *Nat. Commun.* **7**, 11367 (2016).
- [16] J. P. Clancy, A. Lupascu, H. Gretarsson, Z. Islam, *et al.*, *Phys. Rev. B* **89**, 054409 (2014).
- [17] F. Ye, X. Wang, C. Hoffmann, J. Wang, S. Chi, M. Matsuda, B. C. Chakoumakos, J. A. Fernandez-Baca, and G. Cao, *Phys. Rev. B* **92**, 201112 (2015).
- [18] S. J. Yuan, S. Aswartham, J. Terzic, H. Zheng, H. D. Zhao, P. Schlottmann, and G. Cao, *Phys. Rev. B* **92**, 245103 (2015).
- [19] S. Calder, J. W. Kim, G.-X. Cao, C. Cantoni, A. F. May, H. B. Cao, A. A. Aczel, M. Matsuda, Y. Choi, D. Haskel, B. C. Sales, D. Mandrus, M. D. Lumsden, and A. D. Christianson, *Phys. Rev. B* **92**, 165128 (2015).
- [20] A. Glamazda, W.-J. Lee, K.-Y. Choi, P. Lemmens, H. Y. Choi, N. Lee, and Y. J. Choi, *Phys. Rev. B* **89**, 104406 (2014).
- [21] L. J. P. Ament, M. van Veenendaal, T. P. Devereaux, J. P. Hill, and J. van den Brink, *Rev. Mod. Phys.* **83**, 705 (2011).
- [22] J. Kim, D. Casa, M. H. Upton, T. Gog, Y.-J. Kim, J. F. Mitchell, M. Van Veenendaal, M. Daghofer, J. van den Brink, G. Khaliullin, *et al.*, *Phys. Rev. Lett.* **108**, 177003 (2012).
- [23] J. Kim, M. Daghofer, A. H. Said, T. Gog, J. van den Brink, G. Khaliullin, and B. J. Kim, *Nat. Commun.* **5**, 4453 (2014).
- [24] X. Liu, M. P. M. Dean, Z. Y. Meng, M. H. Upton, T. Qi, T. Gog, Y. Cao, J. Q. Lin, D. Meyers, H. Ding, *et al.*, *Phys. Rev. B* **93**, 241102 (2016).
- [25] H. Gretarsson, N. H. Sung, J. Porras, J. Bertinshaw, *et al.*, arXiv:1603.07547 (2016).
- [26] M. P. M. Dean, Y. Cao, X. Liu, S. Wall, D. Zhu, R. Mankowsky, V. Thampy, X. M. Chen, J. G. Vale, D. Casa, *et al.*, *Nat. Mater.* **15**, 601 (2016).
- [27] Further details of the sample growth, sample characterization and density functional calculations are provided

- in the Supplementary Information.
- [28] X. Liu, V. M. Katukuri, L. Hozoi, W.-G. Yin, M. P. M. Dean, M. H. Upton, J. Kim, D. Casa, A. Said, T. Gog, *et al.*, Phys. Rev. Lett. **109**, 157401 (2012).
 - [29] G. Jackeli and G. Khaliullin, Phys. Rev. Lett. **102**, 017205 (2009).
 - [30] B. Vignolle, S. M. Hayden, D. F. McMorrow, H. M. Rønnow, B. Lake, C. D. Frost, and T. G. Perring, Nat. Phys. **3**, 163 (2007).
 - [31] O. J. Lipscombe, S. M. Hayden, B. Vignolle, D. F. McMorrow, and T. G. Perring, Phys. Rev. Lett. **99**, 067002 (2007).
 - [32] M. P. M. Dean, R. S. Springell, C. Monney, K. J. Zhou, J. Pereiro, I. Božović, B. Dalla Piazza, H. M. Rønnow, E. Morenzoni, J. van den Brink, *et al.*, Nat. Mater. **11**, 850 (2012).
 - [33] M. Fujita, H. Hiraka, M. Matsuda, M. Matsuura, J. M. Tranquada, S. Wakimoto, G. Xu, and K. Yamada, J. Phys. Soc. Jpn. **81**, 011007 (2011).
 - [34] W.-G. Yin, X. Liu, A. M. Tsvelik, M. P. M. Dean, M. H. Upton, J. Kim, D. Casa, A. Said, T. Gog, T. F. Qi, G. Cao, and J. P. Hill, Phys. Rev. Lett. **111**, 057202 (2013).
 - [35] W. J. L. Buyers, T. M. Holden, E. C. Svensson, R. A. Cowley, and R. W. H. Stevenson, Phys. Rev. Lett. **27**, 1442 (1971).
 - [36] W. J. L. Buyers, D. E. Pepper, and R. J. Elliott, J. Phys. C Solid State **5**, 2611 (1972).
 - [37] Sophisticated direct simulations of disorder with many large supercells will be published elsewhere.
 - [38] W.-G. Yin, H. Biao, and C.-D. Gong, Phys. Lett. A **220**, 281 (1996).
 - [39] A. de la Torre, S. McKeown Walker, F. Y. Bruno, S. Riccò, Z. Wang, I. Gutierrez Lezama, G. Scheerer, G. Girit, D. Jaccard, C. Berthod, *et al.*, Phys. Rev. Lett. **115**, 176402 (2015).
 - [40] Y. K. Kim, N. H. Sung, J. D. Denlinger, and B. J. Kim, Nat. Phys. **12**, 37 (2016).